Dynamical model of surrogate reactions

Y. Aritomo, S. Chiba, and K. Nishio
Advanced Science Research Center, Japan Atomic Energy Agency, Tokai, Ibaraki 319-1195, Japan
(Received 28 September 2010; revised manuscript received 2 December 2010; published 5 August 2011)

A new dynamical model is developed to describe the whole process of surrogate reactions: Transfer of several nucleons at an initial stage, thermal equilibration of residues leading to washing out of shell effects, and decay of populated compound nuclei are treated in a unified framework. Multidimensional Langevin equations are employed to describe time evolution of collective coordinates with a time-dependent potential energy surface corresponding to different stages of surrogate reactions. The new model is capable of calculating spin distributions of the compound nuclei, one of the most important quantities in the surrogate technique. Furthermore, various observables of surrogate reactions can be calculated, for example, energy and angular distribution of ejectile and mass distributions of fission fragments. These features are important to assess validity of the proposed model itself, to understand mechanisms of the surrogate reactions, and to determine unknown parameters of the model. It is found that spin distributions of compound nuclei produced in $^{18}\mathrm{O} + ^{238}\mathrm{U} \rightarrow ^{16}\mathrm{O} + ^{240*}\mathrm{U}$ and $^{18}\mathrm{O} + ^{236}\mathrm{U} \rightarrow ^{16}\mathrm{O} + ^{238*}\mathrm{U}$ reactions are equivalent and much less than $10\hbar$ and therefore satisfy conditions proposed by Chiba and Iwamoto [Phys. Rev. C **81**, 044604 (2010)] if they are used as a pair in the surrogate ratio method.

DOI: 10.1103/PhysRevC.84.024602 PACS number(s): 24.87.+y, 24.10.−i, 24.60.Ky, 27.90.+b

I. INTRODUCTION

Neutron-induced cross-section data of unstable nuclei are systematically required to design next-generation nuclear facilities such as high-burn-up, fast breeder reactors or accelerator-driven systems for transmutation of nuclear wastes [1]. Such data are also important to understand origin of elements, namely, the *s*- and *r*-process nucleosynthesis (see, e.g., Refs. [2,3]). However, it is not usually possible to measure these cross sections directly by using neutrons owing to difficulty in preparing samples. It is well known that the compound reaction process is the dominant mechanism in the energy region of our interest. Therefore, various experimental methods to measure the "direct" neutron capture components are not applicable to determine them. Instead, other methods are needed, and one promising method is the surrogate reaction approach [4–25]. In this method, (multi)nucleon transfer reactions with an experimentally accessible combination of projectile and target are employed to create the same compound nucleus as the desired neutron reaction, and decay branching ratios to specific channels, normally capture and/or fission, are determined. However, branching ratios are sensitive to the spin and parity of the compound state, while the spin-parity (J^π) distributions of populated nuclei are probably different for the neutron-induced and surrogate reactions. It is well known that if the spin is different by even just 1 unit, the capture branching ratio is totally different for the energy region of our interest. Therefore, the validity of the surrogate method depends on how the difference of the spin-parity distributions is comprehended and compensated properly.

Recently, the surrogate ratio method (SRM) is discussed by Chiba and Iwamoto. It was found that SRM works to a certain accuracy if (1) there exist two surrogate reactions whose spin-parity distributions of decaying nuclei are equivalent and (2) the difference of representative spin values between the neutron-induced and surrogate reactions is not much larger than $10\hbar$, under a condition that (3) a weak Weisskopf-Ewing condition, namely, J^π-by-J^π convergence of the branching ratio, is realized [26]. They form a set of sufficient conditions for the SRM to work. It is important to notice that the J^π distribution may be different even for the neutron-induced and surrogate reactions if these conditions are fulfilled.

The discovery of the above conditions is a great advancement for the whole surrogate technique. Therefore, we need further investigation to verify that the above conditions, especially (1) and (2), which were just assumed in Ref. [26], are really satisfied in certain surrogate reactions. It implies that mechanisms of the surrogate reactions should be understood well. For that aim, it is indispensable to establish a theoretical model to describe the whole process of the surrogate reactions, namely, nucleon transfer and decay of a populated compound nucleus.

In this work, we propose a first version of our model to describe the surrogate reactions based on a theory proposed originally by Zagrebaev and Greiner [27]. This model, called a unified model, can treat the whole reaction processes in heavy- and superheavy-mass regions, which has been applied to several types of reactions [27–31]. The name "unified model" implies an unified dynamical approach and unified multidimensional potential energy. The time-evolution of the system is described by a trajectory calculation on the time-dependent unified potential energy surface using the Langevin equation. Then we treat a two-neutron transfer reaction, $^{18}\mathrm{O} + ^{238}\mathrm{U} \rightarrow ^{16}\mathrm{O} + ^{240}\mathrm{U}$, which is planned to be employed at Japan Atomic Energy Agency (JAEA) as an example of application of the new model to the surrogate reaction. By using the new model, we can obtain various quantities that can be compared with experimental data directly and we can evaluate our theory and determine unknown parameters in the model.

The purpose of this paper is to explain the new model, calculate a fission fragment mass distribution (FFMD) for a

reaction, $^{18}O + ^{238}U$, to calibrate the model parameter, and calculate spin distributions of compound nuclei for the $^{18}O + ^{A}U \rightarrow ^{16}O + ^{A+2*}U$ system, where $A = 236$ and 238, to see if the conditions proposed by Chiba and Iwamoto are satisfied. Here we use the "compound nucleus" for the transfer products [21–23]. In Sec. II, we explain our theoretical framework. The calculation results are presented in Sec. III. In Sec. IV, we present a summary of this study and further discussion.

II. DYNAMICAL MODEL

A. Overview of the model

The surrogate reactions consist of two stages: an initial nucleon transfer process and decay of populated compound nuclei, which have quite different nature to each other. The Hauser-Freshbach (HF) theory [32,33] has been applied to describe the latter part of the surrogate reactions. By the HF theory, we are able to calculate decay branching ratios to specific channels (capture or fission) with arbitrary spin-parity distributions of compound states. However, we cannot predict the spin distribution produced by the initial stage of the surrogate reaction nor the FFMD with the HF theory. For that reason, we need to describe the whole reaction process consistently, that is, starting from the transfer of several nucleons and the decay of the compound nucleus leading to fission, successively. Here we employ a dynamical model, the unified model, to the surrogate reaction.

The unified model was proposed by Zagrebaev and Greiner and was applied to several types of reactions induced by heavy ions [27–31], which include the transfer reactions [30]. An unified dynamical approach and unified multidimensional potential energy are employed in this model, which are the origin of the name of this theory. To apply this model to the surrogate reaction, we extend this model and introduce new procedures. As explained above, the surrogate reactions consist of two processes: the transfer reaction process between a two-body system and decay of the populated compound nuclei (one-body system), for which the masses of the total systems ares very different from each other. Therefore, it is indispensable to connect such different systems to treat surrogate reactions consistently. Evolution of the mass-asymmetry parameter is described by multidimensional Langevin equations without (with) the inertia parameter before (after) the window of the colliding nuclei opens sufficiently. We modify the original unified model [27] also to take account of temperature dependence of the shell correction energy of the potential energy surface.

First, we treat the transfer reaction process within the framework of the unified model. Then we treat the decay of the compound nuclei with an initial condition populated by the former reaction process. We perform a trajectory calculation on a time-dependent potential energy surface corresponding to different stages of the surrogate reaction. A dynamical calculation is carried out in terms of the multidimensional Langevin equation based on the fluctuation-dissipation theorem. By this procedure, we can describe trajectories moving on the potential energy surface, including the nucleon transfer reaction.

We consider in this paper a two-neutron transfer reaction, $^{18}O + ^{238}U \rightarrow ^{16}O + ^{240*}U$, as an example. In the transfer reaction process, we use the potential energy of ^{256}Fm as the total system. After the production of the compound nucleus by the transfer reaction, we then treat the decay of the compound nucleus ^{240}U. In other words, the potential energy surface switches from that of ^{256}Fm to that of ^{240}U as the surrogate reactions proceed from the transfer process to the decay stage.

A schematic picture of our model is presented in Fig. 1. It shows the potential energy surfaces used in the trajectory calculation from the transfer process to the decay of compound nuclei in the reaction $^{18}O + ^{238}U \rightarrow ^{16}O + ^{240}U$. The transfer reaction process is presented in the top left panel of Fig. 1, which shows a diabatic potential energy surface of ^{256}Fm in the z-α ($\delta = 0$) coordinate space. Meanings of these parameters and terms are explained in the next section. The thin arrows correspond to the entrance and the exit channels of two-neutron transfer process. In the calculation, it starts from an infinite distance between the projectile and target, where actually the distance of 30 fm is used. The impact parameters correspond to the relative angular momentum from $\ell = 0$ to $250\hbar$ at intervals of $5\hbar$. Then the calculation stops when the trajectory reaches the distance of 25 fm between the both fragments. We select the two-nucleon transfer among all the events; we select events in which the mass asymmetry parameter α changes from 0.859 corresponding to $^{18}O + ^{238}U$ to 0.875 corresponding to $^{16}O + ^{240}U$.

Next, the decay process of a compound nucleus is presented in the bottom right panel of Fig. 1, which is a potential energy surface of ^{240}U with $\delta = 0.2$ ($\beta_2 \sim 0.2$). The white lines denote mean fission paths. In the decay process, we start the trajectory calculation with the initial condition obtained in the transfer reaction process. As the initial condition, we use the deformation, momentum, angular momentum, and excitation energy of the compound nucleus. These values are different among each trajectory owing to the fluctuation effect in the Langevin equation. The quantities which we can obtain with this calculation are the angular and energy distributions of ejectile, mass and total kinetic energy distributions of fission fragments and neutron multiplicities, and so on. Such quantities can be compared with experimental data directly, which allows us to determine the unknown parameter in the model. In this work, we discuss a mass distribution of fission fragments and determine a value of one of the most uncertain parameters, the sliding friction (see below). In this way, we can evaluate and improve our model step by step by comparing model predictions with experimental data. More details of our model are explained below.

B. Potential energy surface

The initial stage of the surrogate reaction consists of two parts: (1) a fast diabatic part in which the reaction proceeds too fast for nucleons to reconfigure their single-particle states so the system goes through the ground-state configurations of the target and projectile and (2) a part where the system relaxes to the ground state of the total composite system, which changes the potential energy surface to an adiabatic one. Therefore, we take into account time evolution of the potential energies from the diabatic one $V_{\rm diab}(q)$ to the adiabatic one $V_{\rm adiab}(q)$;

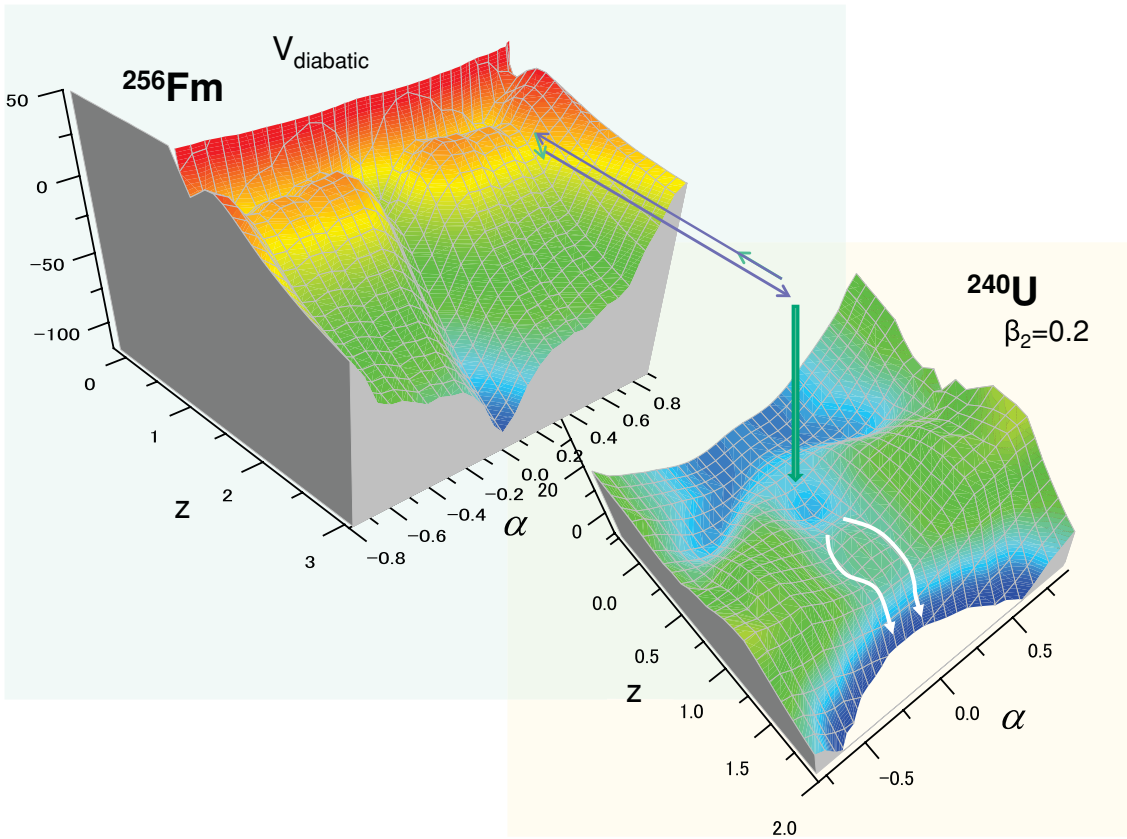

FIG. 1. (Color online) Schematic picture of the calculation. For the surrogate reaction $^{18}\mathrm{O} + ^{238}\mathrm{U} \rightarrow ^{16}\mathrm{O} + ^{240}\mathrm{U}$, the potential energy surfaces from the transfer reaction to the decay process of compound nuclei are presented. The transfer reaction is shown in the left panel, which is the diabatic potential energy surface of ^{256}Fm in the $z - \alpha(\delta = 0)$ coordinate space. The decay process of compound nucleus is presented in the right panel, which is the adiabatic potential energy surface of ^{240}U with $\delta = 0.2$ ($\beta_2 \sim 0.2$).

here q denotes a set of collective coordinates representing the nuclear deformation. The diabatic potential is calculated by a folding procedure with effective nucleon-nucleon interaction [27,28,34], which is shown in the top left panel of Fig. 1. We can see a "potential wall" in the overlap region of the colliding system, which corresponds to a hard core representing incompressibility of nuclear matter. However, the adiabatic potential energy of the system is calculated using an extended two-center shell model [34]. We then connect the diabatic and adiabatic potentials with a time-dependent weighting function as follows:

$$V = V_{\mathrm{diab}}(q) f(t) + V_{\mathrm{adiab}}(q)[1 - f(t)],$$
$$f(t) = \exp\left(-\frac{t}{\tau}\right). \quad (1)$$

Here t is the time of interaction and $f(t)$ is the weighting function with the relaxation time τ. We use a relaxation time $\tau = 10^{-21}$ s, which was suggested in Ref. [35]. It is empirically known that calculated results do not depend noticeably on the relaxation time.

As the coordinates to express nuclear deformation, we use the two-center parametrization [36,37]. To solve the dynamical equation numerically and to avoid the huge computing time, we restrict the number of degrees of freedom and employ three parameters as follows: z_0 (distance between centers of two potentials), δ (deformation of fragments), and α (mass asymmetry of the colliding nuclei); $\alpha = (A_1 - A_2)/(A_1 + A_2)$, where A_1 and A_2 denote the mass numbers of the target and the projectile, respectively [27,38]. Later on, A_1 and A_2 are used to denote mass numbers of two fission fragments.

The parameter δ is defined as $\delta = 3(a - b)/(2a + b)$, where a and b denote the half length of the axes of ellipse in the z_0 and ρ directions, respectively, as expressed in Fig. 1 in Ref. [36]. We assume that each fragment has the same deformations as a first step. Furthermore, we use scaling to save computation time and employ a coordinate z defined as $z = z_0/(R_{\mathrm{CN}} B)$, where R_{CN} denotes the radius of the spherical compound nucleus. The parameter B is defined as $B = (3 + \delta)/(3 - 2\delta)$.

In the two-center parametrization, the neck parameter is denoted by ϵ and is known to be different in the entrance and exit channels [34]. Therefore, we employ $\epsilon = 1$ for the entrance channel and $\epsilon = 0.35$ for the exit channel to describe a realistic nuclear shape. We introduce a time-dependent potential energy surface in terms of ϵ using a relaxation time for ϵ of $\tau_\epsilon = 10^{-20}$ s [39] as follows:

$$V_{\mathrm{adiab}} = V_{\mathrm{adiab}}(q, \epsilon = 1) f_\epsilon(t) + V_{\mathrm{adiab}}(q, \epsilon = 0.35)[1 - f_\epsilon(t)],$$
$$f_\epsilon(t) = \exp\left(-\frac{t}{\tau_\epsilon}\right). \quad (2)$$

It roughly corresponds to the values of ϵ parameter which minimize the potential energy surface during fusion-fission process.

C. Dynamical equations

We then perform trajectory calculations on the time-dependent unified potential energy using the Langevin equation [27,28,38].

The nucleon transfer for slightly separated nuclei is important in surrogate reactions. Such intermediate nucleon exchange plays an important role in the fusion process at incident energies near and below the Coulomb barrier as well. We treat the nucleon transfer using the procedure described in Refs. [27,28]:

$$\frac{d\alpha}{dt} = \frac{2}{A_{\rm CN}} D_A^{(1)}(\alpha) + \frac{2}{A_{\rm CN}} \sqrt{D_A^{(2)}(\alpha)\gamma_\alpha(t)}. \tag{3}$$

This is a Langevin equation neglecting inertia mass for the mass asymmetry parameter. It expresses change of the asymmetry parameter α owing to drift (first term on the right-hand side) and diffusion (second term on the right-hand side) processes. It is obtained by a certain approximation starting from the master equation for transition of different particle-hole states. Such a master equation giving discrete change of nucleon numbers is transformed to an equation for a continuous variable α via Fokker-Planck equation to the Langevin equation shown above [27,28].

Though the N/Z equilibrium affects the transfer process, in the present model we assume that the N/Z equilibrium is achieved quickly as a first approximation, using the same model in the reference [27]. We plan to introduce the charge asymmetry and the neutron number asymmetry in the next study, instead of the mass asymmetry parameter.

After the window of the touching nuclei opens sufficiently (hereafter "the mononucleus state"), the treatment of the evolution of the mass-asymmetric parameter α switches from Eq. (3) to the Langevin equations with the procedure described in Ref. [38]. Here we assume that the condition for the mononucleus is realized when the trajectory enters into the region $z < 1.2$.

The multidimensional Langevin equations [27,31,38] are now unified as

$$\begin{aligned}
\frac{dq_i}{dt} &= (m^{-1})_{ij} p_j, \\
\frac{dp_i}{dt} &= -\frac{\partial V}{\partial q_i} - \frac{1}{2}\frac{\partial}{\partial q_i}(m^{-1})_{jk} p_j p_k - \gamma_{ij}(m^{-1})_{jk} p_k \\
&\quad + g_{ij} R_j(t), \\
\frac{d\theta}{dt} &= \frac{\ell}{\mu_R R^2}, \quad \frac{d\varphi_1}{dt} = \frac{L_1}{\Im_1}, \quad \frac{d\varphi_2}{dt} = \frac{L_2}{\Im_2}, \\
\frac{d\ell}{dt} &= -\frac{\partial V}{\partial \theta} - \gamma_{\rm tan}\left(\frac{\ell}{\mu_R R} - \frac{L_1}{\Im_1}a_1 - \frac{L_2}{\Im_2}a_2\right) R \\
&\quad + R g_{\rm tan} R_{\rm tan}(t), \\
\frac{dL_1}{dt} &= -\frac{\partial V}{\partial \varphi_1} + \gamma_{\rm tan}\left(\frac{\ell}{\mu_R R} - \frac{L_1}{\Im_1}a_1 - \frac{L_2}{\Im_2}a_2\right) a_1 \\
&\quad - a_1 g_{\rm tan} R_{\rm tan}(t),
\end{aligned}$$

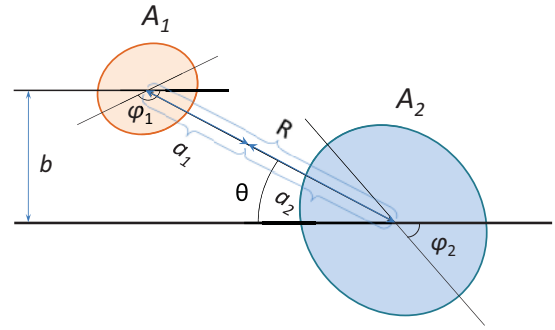

FIG. 2. (Color online) Definition of parameters used in the model.

$$\begin{aligned}
\frac{dL_2}{dt} &= -\frac{\partial V}{\partial \varphi_2} + \gamma_{\rm tan}\left(\frac{\ell}{\mu_R R} - \frac{L_1}{\Im_1}a_1 - \frac{L_2}{\Im_2}a_2\right) a_2 \\
&\quad - a_2 g_{\rm tan} R_{\rm tan}(t),
\end{aligned} \tag{4}$$

where a summation over repeated indices is assumed. The collective coordinates q_i stand for z, δ, and α. The symbol p_i denotes momentum conjugate to q_i, and V is the multidimensional potential energy. A definition of other parameters is given in Fig. 2: The symbols θ and ℓ are the relative orientation of nuclei and relative angular momentum, respectively, φ_1 and φ_2 denote the angles of rotation of the nuclei in the reaction plane (their moments of inertia and angular momenta are $\Im_{1,2}$ and $L_{1,2}$, respectively), $a_{1,2} = R/2 \pm (R_1 - R_2)/2$ are the distances from the centers of the fragments up to the middle point between nuclear surfaces, and $R_{1,2}$ are the nuclear radii. The symbol R is the distance between the nuclear centers. The total angular momentum $L = \ell + L_1 + L_2$ is conserved. The symbol μ_R denotes the reduced mass, and $\gamma_{\rm tan}$ is the friction force in the tangential direction of colliding nuclei; here we call it the sliding friction. For separated nuclei the phenomenological nuclear friction forces are denoted by γ_R^F and $\gamma_{\rm tan}^F$ for the radial and the sliding friction, with the Woods-Saxon radial form factor as described in Refs. [27,28].

The radial and sliding frictions are described as $\gamma_R^F = \gamma_R^0 F(\zeta)$, $\gamma_{\rm tan} = \gamma_t^0 F(\zeta)$, where the radial form factor $F(\zeta) = (1 + \mathrm{e}^{\zeta})^{-1}$, $\zeta = (\xi - \rho_F)/a_F$. γ_R^0 and γ_t^0 denote the strength of the radial and the tangential frictions, respectively. $\rho_F \sim 2$ fm and $a_F \sim 0.6$ fm are the model parameters, and ξ is the distance between nuclear surface $\xi = R - R_{\rm contact}$, where $R_{\rm contact} = R_1 + R_2$ [27].

The symbols m_{ij} and γ_{ij} stand for elements of the shape-dependent collective inertia and friction tensors, respectively. For separated nuclei, we use the reduced mass and the phenomenological friction forces γ_R^F. Then we switch the phenomenological friction to the friction for mononuclear system using a smoothing function $\theta(\xi) = (1 + \exp^{-\xi/0.3})^{-1}$ [27,28]. For the mononuclear system, the wall-and-window one-body dissipation $\gamma_R^{\rm one}$ is adopted for the friction tensor [40–47]. The absolute values of the wall-and-window dissipation for the radial direction γ_{zz}, the deformation $\gamma_{\delta\delta}$ and the mass asymmetry $\gamma_{\alpha\alpha}$ as function of collective variable z with $\delta = 0$, $\alpha = 0$, and $\epsilon = 0.35$ for ^{256}Fm are illustrated in Fig. 3.

The resulting radial friction is expressed as $\gamma_R = \gamma_R^{\rm one} + \theta(\xi)\gamma_R^F(\xi - \rho)$, which is related to γ_{zz}. A hydrodynamical

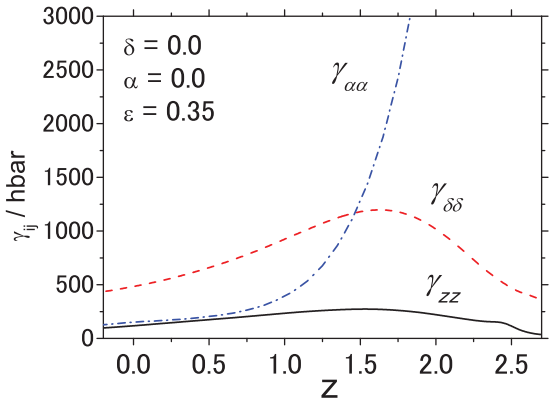

FIG. 3. (Color online) The absolute values of the wall-and-window dissipation for the radial direction γ_{zz}, the deformation $\gamma_{\delta\delta}$, and the mass asymmetry $\gamma_{\alpha\alpha}$ as function of collective variables z with $\delta = 0$, $\alpha = 0$, and $\epsilon = 0.35$ for ^{256}Fm.

inertia tensor m_{ij} is adopted in the Werner-Wheeler approximation for the velocity field [48]. Figure 4 shows the absolute values of the inertia tensor for the radial direction m_{zz}, the deformation $m_{\delta\delta}$, and the mass asymmetry $m_{\alpha\alpha}$ as function of collective variables z with $\delta = 0$, $\alpha = 0$, and $\epsilon = 0.35$ for ^{256}Fm.

The normalized random force $R_i(t)$ is assumed to be of white noise, that is, $\langle R_i(t)\rangle = 0$ and $\langle R_i(t_1)R_j(t_2)\rangle = 2\delta_{ij}\delta(t_1 - t_2)$. The strength of the random force g_{ij} is given by the Einstein relation, $\gamma_{ij}T = \sum_k g_{ij}g_{jk}$, where T is the temperature of the compound nucleus calculated from the intrinsic energy of the composite system.

The adiabatic potential energy is defined as

$$V_{\rm adiab}(q, L, T) = V_{\rm LD}(q) + \frac{\hbar^2 L(L+1)}{2I(q)} + V_{\rm SH}(q, T), \quad (5)$$

$$V_{\rm LD}(q) = E_S(q) + E_C(q), \quad (6)$$

$$V_{\rm SH}(q, T) = E^0_{\rm shell}(q)\Phi(T), \quad (7)$$

$$\Phi(T) = \exp\left(-\frac{E^*}{E_d}\right), \quad (8)$$

where $I(q)$ stands for the moment of inertia of a rigid body with deformation q, and $V_{\rm LD}$ and $V_{\rm SH}$ are the potential energy of the

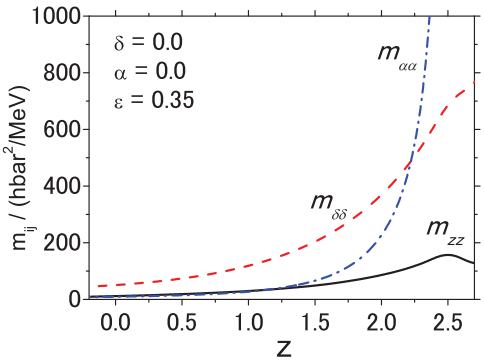

FIG. 4. (Color online) The absolute values of the inertia tensor for the radial direction m_{zz}, the deformation $m_{\delta\delta}$ and the mass asymmetry $m_{\alpha\alpha}$ as function of collective variables z with $\delta = 0$, $\alpha = 0$, and $\epsilon = 0.35$ for ^{256}Fm.

finite-range liquid drop model and the shell correction energy taking into account the temperature dependence, respectively. The symbol $E^0_{\rm shell}$ denotes the shell correction energy at $T = 0$. The temperature-dependent factor $\Phi(T)$ is discussed in Ref. [49], where E^* denotes the excitation energy of the compound nucleus. The shell damping energy E_d is chosen as 20 MeV, which is given by Ignatyuk *et al.* [50].

The symbols E_S and E_C denote a generalized surface energy [51] and Coulomb energy, respectively. The centrifugal energy arising from the angular momentum L of the rigid body is also considered. The intrinsic energy of the composite system $E_{\rm int}$ is calculated for each trajectory as

$$E_{\rm int} = E^* - \tfrac{1}{2}(m^{-1})_{ij}p_i p_j - V(q, L, T). \quad (9)$$

Here E^* is given by $E^* = E_{\rm c.m.} - Q$, where Q and $E_{\rm c.m.}$ denote the Q value of the reaction and the incident energy in the center-of-mass frame, respectively. Each trajectory starts from a sufficiently large distance between both nuclei [31].

D. Computation

Owing to the difference of the initial impact parameters (or the different initial relative angular momenta), various kind of reaction processes can occur. Moreover, even when the trajectories start with the same initial impact parameter, reactions proceed in quite different ways owing to the random force in the dynamical equation, which finally leads to different reaction channels. By choosing various impact parameters randomly and giving proper weights, whole processes of reactions are described by the present model: the elastic and inelastic scattering, deep inelastic collision, quasifission, fusion-fission process, and a few nucleon transfer process (the surrogate reaction). They are treated simultaneously by the model. This is a big advantage of the present approach; because these reactions correlate, they can give information to each other. An example is a determination of the unknown parameter γ_t^0 through FFMD of fusion-fission-like process as is discussed below.

III. RESULTS AND DISCUSSION

The unified model, on which the present model is based, has been applied to several types of reactions and succeeded in describing the experimental data [27–31]. For the transfer channel, the model has applied to multinucleon transfer reactions ^{58}Ni + ^{208}Pb at $E_{\rm lab} = 328.4$ MeV and ^{82}Se + ^{238}U at $E_{\rm lab} = 500$ MeV, and compared with the experimental data [30]. Figure 10(c) in Ref. [27] showed the charge distributions of the projectilelike fragment obtained in the ^{136}Xe + ^{209}Bi reaction at $E_{\rm c.m.} = 861$ MeV. The calculations agree with the experimental data; few nucleon transfers show especially good agreement. In our previous study, we precisely investigated the incident energy dependence of mass distribution of fission fragments in the reactions ^{36}S + ^{238}U and ^{30}Si + ^{238}U [31,52,53]. The calculation results reproduced the experimental data well and clarified the origin of the fine structure of the mass distribution of fission fragments at the low incident energy.

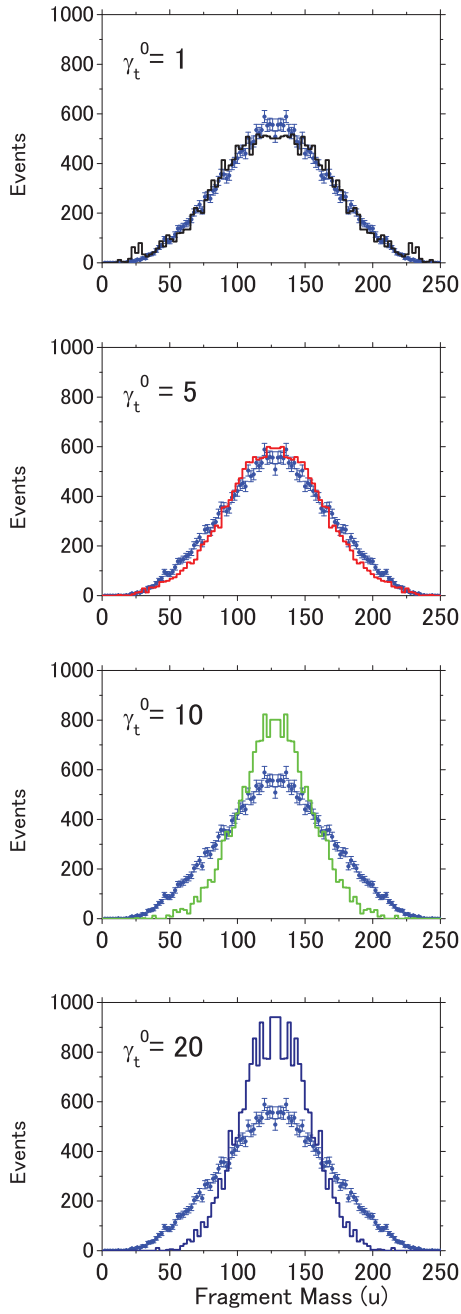

FIG. 5. (Color online) Fragment mass distribution obtained in the reaction $^{18}O + ^{238}U$ at an incident energy of $E_{c.m.} = 133.5$ MeV. Experimental data and calculation results are denoted by circles and histograms, respectively. Calculations are shown with sliding frictions $\gamma_t^0 = 1$, 5, 10, and 20×10^{-22} MeV s fm^{-2}, which are multiplied by the factor such that the total cross section agrees with the experimental value to compare the shape of the mass distribution with the experiment.

Here we apply the present model to the surrogate reaction. To evaluate and clarify the model, we focus on the mass distribution of the fission fragments and compare calculated results with experimental data. Furthermore, we investigate spin distributions of the compound nucleus populated by transfer reactions and discuss the validity condition of the SRM [26]. We choose a system of $^{18}O + ^{A}U \rightarrow ^{16}O + ^{A+2*}U$ reaction, where $A = 236$ or/and 238.

In the Langevin calculation, the sliding friction is mainly responsible for the dissipation of the angular momentum [54,55], though its value is uncertain. In the present work, we treat the sliding friction as a parameter of the model and investigate dependence of the calculation upon this parameter. Measured FFMD data in the reaction $^{18}O + ^{238}U$ at $E_{c.m.} = 133.5$ MeV is shown by dots in Fig. 5. The experimental setup to measure the FFMD and the data analysis are nearly the same as in Refs. [52,56]. In the experiment, both fission fragments were detected in coincidence by using position-sensitive multiwire proportional counters (MWPCs). The difference of the setup from the references [52,56] was the angles of the detector positions that MWPC1 and MWPC2 were located at -90° and $+90^\circ$ with respect to the beam direction. The mass distributions were obtained from the events that the momentum of the projectile was fully transferred to the composite system (full momentum transfer) by constructing the the folding angle.

In Fig. 5, calculated data with $\gamma_t^0 = 1, 5, 10$ and 20×10^{-22} MeV s fm^{-2} are denoted by the black, red, green, and dark blue histograms, respectively. Here, for the two-body region, we used the strength parameter of nuclear friction $\gamma_R^0 = 20 \times 10^{-22}$ MeV s fm^{-2} (see p. 834 of Ref. [27]), which is almost equivalent to the two-body friction γ_R^{WW} with nuclear viscosity $\mu_0 = 0.20 \times 10^{-22}$ MeV s fm^{-3} near the contact point in this system. It is clearly seen that the result with $\gamma_t^0 = 5 \times 10^{-22}$ MeV s fm^{-2} reproduces the experimental data very well. With larger sliding friction, the variance of results becomes smaller.

Then calculations for the two-neutron transfer reaction are carried out without adjustable parameters. From such calculations, we can determine spin distributions of the surrogate reactions $^{18}O + ^{236}U \rightarrow ^{16}O + ^{238*}U$ and $^{18}O + ^{238}U \rightarrow ^{16}O + ^{240*}U$ and verify if the two assumptions proposed by Chiba and Iwamoto [26]—namely, (1) there exist two surrogate reactions whose spin-parity distributions of decaying nuclei are almost equivalent, and (2) difference of representative spin values

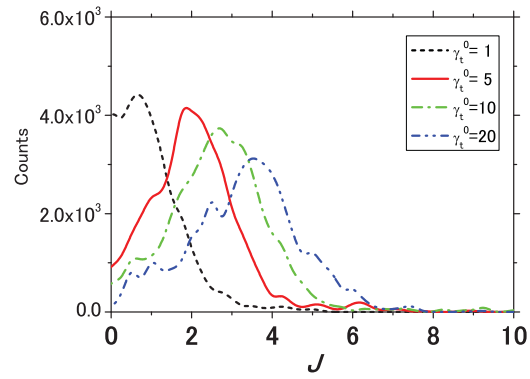

FIG. 6. (Color online) Spin distribution of compound nucleus ^{240}U in the reaction $^{18}O + ^{238}U \rightarrow ^{16}O + ^{240}U$ at the incident energy of $E_{c.m.} = 133.5$ MeV for several sliding frictions. The black, red, green and blue lines denote for $\gamma_t^0 = 1$, 5, 10, and 20×10^{-22} MeV s fm^{-2}, respectively.

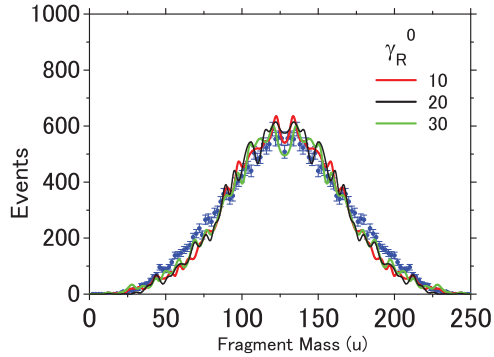

FIG. 7. (Color online) Mass distribution in the reaction $^{18}\mathrm{O} + ^{238}\mathrm{U}$ at the incident energy of $E_{\mathrm{c.m.}} = 133.5$ MeV. Experimental data and calculation results are denoted by circles and lines, respectively. Calculations are used the phenomenological friction γ_R^F at $\gamma_R^0 = 10$, 20, and 30×10^{-22} MeV s fm^{-2}, which are denoted by the red, black, and green lines, respectively. Sliding friction $\gamma_t^0 = 5 \times 10^{-22}$ MeV s fm^{-2} is used.

between the neutron-induced and surrogate reactions is not much larger than $10\hbar$—are really satisfied.

Figure 6 shows calculated spin distributions of compound nucleus $^{240}\mathrm{U}$ populated in the reaction $^{18}\mathrm{O} + ^{238}\mathrm{U} \rightarrow ^{16}\mathrm{O} + ^{240}\mathrm{U}$ at an incident energy of $E_{\mathrm{c.m.}} = 133.5$ MeV. Results with various values of the sliding friction are shown. The black, red, green, and blue lines denote for $\gamma_t^0 = 1$, 5, 10, and 20×10^{-22} MeV s fm^{-2}, respectively. We can see that the majority of the spin of compound nucleus is much less than $10\hbar$ for each value of the sliding friction although they diverge depending on γ_t^0. Therefore, it is important for the model to have a capability to determine values of unknown parameters, as shown above. Our model is particularly powerful because this parameter is determined by using observables corresponding to other reaction channels, which can be treated simultaneously with the surrogate reactions of our interest.

We demonstrate the sensitivity of the spin and mass distributions to the several strengths of radial friction in the

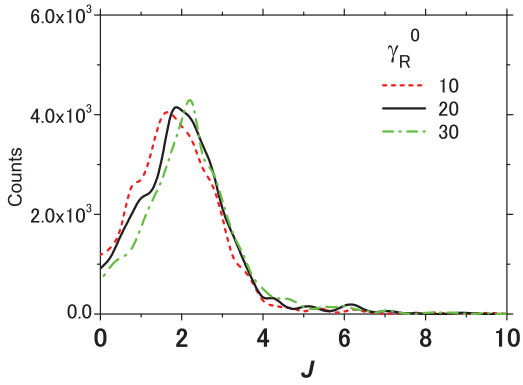

FIG. 8. (Color online) Spin distribution of compound nucleus $^{240}\mathrm{U}$ in the reaction $^{18}\mathrm{O} + ^{238}\mathrm{U} \rightarrow ^{16}\mathrm{O} + ^{240}\mathrm{U}$ at the incident energy of $E_{\mathrm{c.m.}} = 133.5$ MeV for the several phenomenological friction γ_R^F. Calculations are used the phenomenological friction γ_R^F at $\gamma_R^0 = 10$, 20, and 30×10^{-22} MeV s fm^{-2}. The lines denote the same items those in Fig. 7. Sliding friction $\gamma_t^0 = 5 \times 10^{-22}$ MeV s fm^{-2} is used.

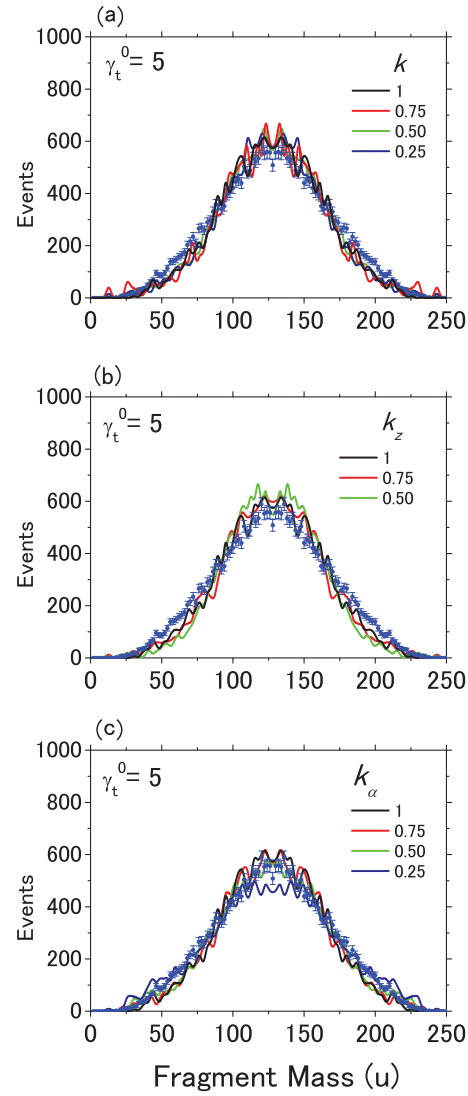

FIG. 9. (Color online) Fragment mass distribution obtained in the reaction $^{18}\mathrm{O} + ^{238}\mathrm{U}$ at an incident energy of $E_{\mathrm{c.m.}} = 133.5$ MeV. Experimental data and calculation results are denoted by circles and lines, respectively. (a) Calculations are shown with reduction factor k to the wall-and-window friction in $k = 1$, 0.75, 0.50, and 0.25; (b) with reduction factor k_z to zz component in $k_z = 1$, 0.75, and 0.50; and (c) with reduction factor k_α to $\alpha\alpha$ component in $k_\alpha = 1$, 0.75, 0.50, and 0.25. Sliding friction $\gamma_t^0 = 5 \times 10^{-22}$ MeV s fm^{-2} is used.

two-body region. Figure 7 shows the mass distribution in the reaction $^{18}\mathrm{O} + ^{238}\mathrm{U} \rightarrow ^{16}\mathrm{O} + ^{240}\mathrm{U}$ at the incident energy of $E_{\mathrm{c.m.}} = 133.5$ MeV. Experimental data and calculation results are denoted by circles and lines, respectively. Calculations are used the phenomenological friction γ_R^F at $\gamma_R^0 = 10$, 20, and 30×10^{-22} MeV s fm^{-2}, which are denoted by the red, black, and green lines, respectively. The spin distributions of this system are shown in Fig. 8. The lines denote the same items as those in Fig. 7.

In mononucleus region, we used the reduction factor k for the wall-and-window formula [47]. Also, we used the reduction factor for the z direction and the α direction,

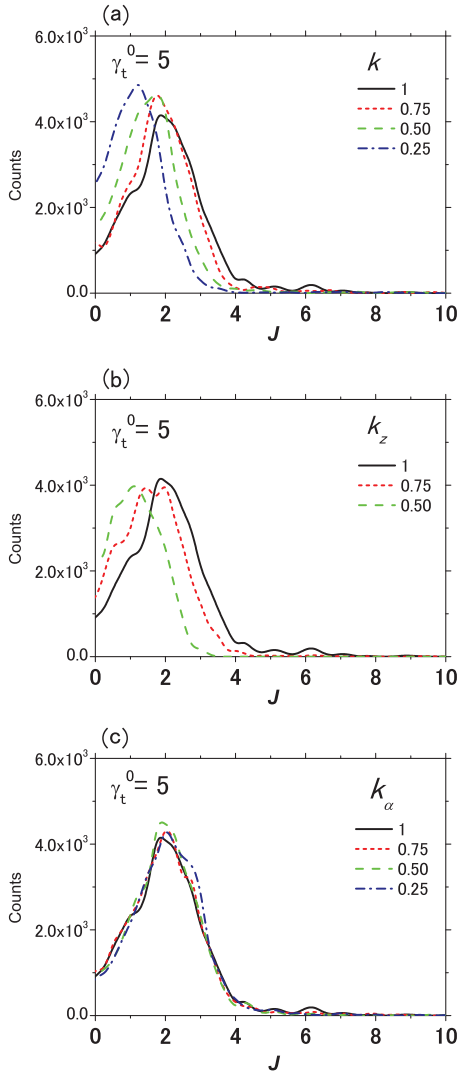

FIG. 10. (Color online) Spin distribution of compound nuclei ^{240}U in the reaction $^{18}\mathrm{O} + ^{238}\mathrm{U} \rightarrow ^{16}\mathrm{O} + ^{240}\mathrm{U}$ at an incident energy of $E_{\mathrm{c.m.}} = 133.5$ MeV. The lines denote the same items those in Fig. 9. Sliding friction $\gamma_t^0 = 5 \times 10^{-22}$ MeV s fm^{-2} is used.

independently, which are denoted by k_z and k_α, respectively. The mass and spin distributions with several k, k_z, and k_α are shown in Figs. 9 and 10, respectively. Figure 9 shows the fragment mass distribution obtained in the reaction $^{18}\mathrm{O} + ^{238}\mathrm{U}$ at an incident energy of $E_{\mathrm{c.m.}} = 133.5$ MeV. Experimental data and calculation results are denoted by circles and lines, respectively. Figure 9(a) shows the calculations with the reduction factor k to the wall-and-window friction in $k = 1$, 0.75, 0.50, and 0.25, which are denoted by the black, red, green, and dark blue lines, respectively. The calculations with the reduction factor k_z in $k_z = 1$, 0.75, and 0.50 are shown in Fig. 9(b), which are denoted by the black, red, and green lines, respectively. In Fig. 9(c), the calculations with k_α in $k_\alpha = 1$, 0.75, 0.50, and 0.25 are denoted by the black, red, green, and dark blue lines, respectively. Figure 10 shows the spin distributions with several reduction factors, which lines denote the same items as those in Fig. 9. The main futures of mass and spin distributions do not change so much for the

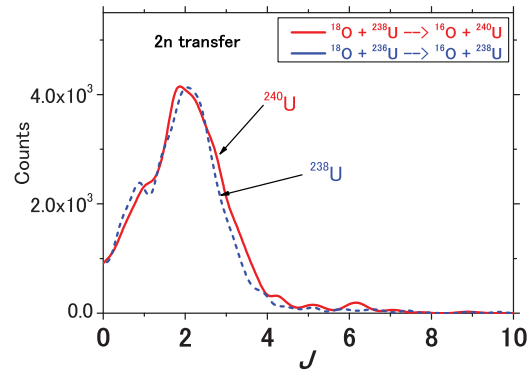

FIG. 11. (Color online) Spin distribution of compound nuclei ^{240}U and ^{238}U in the transfer reactions $^{18}\mathrm{O} + ^{238}\mathrm{U} \rightarrow ^{16}\mathrm{O} + ^{240}\mathrm{U}$ and $^{18}\mathrm{O} + ^{236}\mathrm{U} \rightarrow ^{16}\mathrm{O} + ^{238}\mathrm{U}$ at the incident energy of $E_{\mathrm{c.m.}} = 133.5$ MeV, respectively. Sliding friction $\gamma_t^0 = 5 \times 10^{-22}$ MeV s fm^{-2} is used.

friction with several reduction factors. This is a case where the incident energy is rather high ($E_{\mathrm{c.m.}} = 133$ MeV). As shown in Figs. 5 and 6, the sliding friction has much effect on the mass and spin distribution in this system.

Figure 11 shows spin distributions of compound nuclei ^{240}U and ^{238}U in the transfer reactions $^{18}\mathrm{O} + ^{238}\mathrm{U} \rightarrow ^{16}\mathrm{O} + ^{240}\mathrm{U}$ and $^{18}\mathrm{O} + ^{236}\mathrm{U} \rightarrow ^{16}\mathrm{O} + ^{238}\mathrm{U}$ at an incident energy of $E_{\mathrm{c.m.}} = 133.5$ MeV, respectively, with the sliding friction $\gamma_t^0 = 5 \times 10^{-22}$ MeV s fm^{-2}. These distributions should be interpreted as a semiclassical estimate of a spin distribution corresponding to excitation of rotational motion owing to angular momentum transfer occurring in these reactions. It is easily noticed that the spin distributions of the compound nuclei populated by the two reactions are almost equivalent. These results suggest that assumptions (1) and (2) shown above for the SRM to work [26] are proved to be correct within this model. In conjunction with the weak Weisskopf-Ewing condition proposed in Ref. [26] (which can be verified by Hauser-Feshbach theory), the present result suggests that $^{18}\mathrm{O} + ^{238}\mathrm{U} \rightarrow ^{16}\mathrm{O} + ^{240}\mathrm{U}$ and $^{18}\mathrm{O} + ^{236}\mathrm{U} \rightarrow ^{16}\mathrm{O} + ^{238}\mathrm{U}$ reactions can be employed as a pair in the SRM.

In the calculation, we obtain the production cross sections for ^{240}U in the transfer reaction $^{18}\mathrm{O} + ^{238}\mathrm{U} \rightarrow ^{16}\mathrm{O} + ^{240}\mathrm{U}$ at an incident energy of $E_{\mathrm{c.m.}} = 133.5$ MeV as 11.35 mb for $\gamma_t^0 = 5 \times 10^{-22}$ MeV s fm^{-2}. The mode of the excitation energy of ^{240}U is 13.5 MeV. This information will be useful in performing the experiments.

We propose that this model is a powerful and useful tool to describe the surrogate reaction process, even though it is a semiclassical model. To describe the transfer reaction process more accurately, we may have to consider quantum effects precisely. Quantum mechanical models such as DWBA or CDCC [57] would be more appropriate to describe the nucleon-transfer part of the surrogate reactions. Moreover, new model based on a microscopic stochastic mean-field (SMF) approach would be applied [58–60]. It will be absolutely necessary if we use light-ion projectiles. We can use these sophisticated models if they are available and connect the populated spin-distribution to the later part of the present model. However, it is difficult to treat transition probabilities

to continuous levels quantum mechanically as realized in surrogate reactions. As the first step, therefore, we try to understand the gross feature of the surrogate reaction and analyze the reaction mechanism using the present model in this paper. It is especially known that the dynamical model is useful to discuss the mass distribution of fission fragments [61,62], an important observable of the surrogate reactions that contains information on the populated compound nuclei such as the spin distribution [63].

IV. SUMMARY

We propose a first version of a unified dynamical theory to describe the whole process of surrogate reactions; the nucleon transfer, thermalization, and the decay of the populated compound nuclei. To realize it, we introduced new procedures to the unified theory of Zagrebaev and Greiner, namely, switching of the potential energy surfaces having very different mass numbers, Langevin equations depending on different stages of the reaction, and a temperature-dependent shell correction energy. Trajectory calculations in terms of the Langevin equations are employed on a time-dependent potential energy surface corresponding to different stages of the surrogate reactions. After the transfer process, decay of the populated compound nucleus is calculated with the initial condition obtained from the preceding transfer process. This model can yield many observables which can be compared with experimental data directly.

As an example of the application of the present model to surrogate reactions, we considered a two-nucleon transfer reaction, $^{18}\mathrm{O} + ^{238}\mathrm{U} \rightarrow ^{16}\mathrm{O} + ^{240}\mathrm{U}$, which is planned to be performed at JAEA. We treated the sliding friction as a parameter of the model and discussed the dependence of the calculation results upon the sliding friction. Then we discussed the validity condition of the SRM. We calculated the spin distribution of the compound nuclei with several sliding frictions for the compound nucleus $^{240}\mathrm{U}$ in the reaction $^{18}\mathrm{O} + ^{238}\mathrm{U} \rightarrow ^{16}\mathrm{O} + ^{240}\mathrm{U}$ at the incident energy of $E_{\mathrm{c.m.}} = 133.5$ MeV. The calculation results showed that the spin of compound nucleus was less than $10\hbar$ for each value of the sliding friction. Finally, we discussed spin distributions of compound nucleus $^{240}\mathrm{U}$ and $^{238}\mathrm{U}$ in the transfer reactions $^{18}\mathrm{O} + ^{238}\mathrm{U} \rightarrow ^{16}\mathrm{O} + ^{240}\mathrm{U}$ and $^{18}\mathrm{O} + ^{236}\mathrm{U} \rightarrow ^{16}\mathrm{O} + ^{238}\mathrm{U}$, respectively. It was found that the spin distributions of decaying nuclei populated by the two reactions are almost equivalent. Therefore, it is concluded that if these reactions are used as a pair in the SRM, they would yield the correct neutron cross sections [26]. These calculation results suggested validity of the SRM within this model.

In the present model, however, nuclei were treated as nuclear matter, and a semiclassical approach was employed except for the fact that we took into account the shell correction energy on the potential energy surface. Such semiclassical model may be too simple, and we may have to consider quantum effects to describe the reactions more accurately. Nevertheless, the present model is flexible enough to take account of results of more elaborated models. We therefore consider that the present model is capable enough, as a first step, to understand gross features of the surrogate reactions which itself is already quite complicated.

As further studies, we hope to improve the model in the nucleon transfer part by taking into account the quantum effect more precisely. We will employ the quantum mechanical models such as DWBA, CDCC [57], or SMF [58–60]. We plan to introduce the charge asymmetry and the neutron number asymmetry instead of the mass asymmetry. After experiments of the surrogate reaction at JAEA are performed, we can compare model predictions with experimental data, for example, distributions of emission angle and energy loss of ejectile, mass, charge, and total kinetic energy distributions of fission fragments from various exclusive fission channels, and the model will be upgraded successively.

ACKNOWLEDGMENTS

The authors are grateful to Professor V. I. Zagrevaev, Dr. A.V. Karpov and Dr. F. A. Ivanyuk for helpful suggestions and valuable discussion. The special thanks are deserved to Dr. S. Hashimoto for his helpful comments. The diabatic potential and adiabatic potential were calculated using the NRV code [34]. A part of the numerical calculations was carried out on SX8 at YITP in Kyoto University. The present study is the result of "Development of a Novel Technique for Measurement of Nuclear Data Influencing the Design of Advanced Fast Reactors" entrusted to Japan Atomic Energy Agency (JAEA) by the Ministry of Education, Culture, Sports, Science and Technology of Japan (MEXT).

[1] International Atomic Energy Agency, eds., *Fission Product Yield Data for the Transmutation of Minor Actinide Nuclear Waste* (IAEA, Vienna, 2008).
[2] D. Arnett, *Supernovae and Nucleosynthesis* (Princeton University Press, Princeton, NJ, 1996).
[3] B. E. J. Pagel, *Nucleosynthesis and Chemical Evolution of Galaxies* (Cambridge University Press, Cambridge, 1997).
[4] J. D. Cramer and H. C. Britt, Phys. Rev. C **2**, 2350 (1970).
[5] J. D. Cramer and H. C. Britt, Nucl. Sci. Eng. **41**, 177 (1970).
[6] B. B. Back, O. Hansen, H. C. Britt, and J. D. Garrett, Phys. Rev. C **9**, 1924 (1974).
[7] B. B. Back, H. C. Britt, O. Hansen, B. Leroux, and J. D. Garrett, Phys. Rev. C **10**, 1948 (1974).
[8] H. C. Britt and J. B. Wilhelmy, Nucl. Sci. Eng. **72**, 222 (1979).
[9] W. Younes and H. C. Britt, Phys. Rev. C **67**, 024610 (2003).
[10] W. Younes and H. C. Britt, Phys. Rev. C **68**, 034610 (2003).
[11] M. Petit *et al.*, Nucl. Phys. A **735**, 347 (2004).
[12] C. Plettner *et al.*, Phys. Rev. C **71**, 051602(R) (2005).
[13] S. Boyer *et al.*, Nucl. Phys. A **775**, 175 (2006).
[14] J. T. Burke *et al.*, Phys. Rev. C **73**, 054604 (2006).
[15] J. E. Escher and F. S. Dietrich, Phys. Rev. C **74**, 054601 (2006).
[16] B. F. Lyles *et al.*, Phys. Rev. C **76**, 014606 (2007).

[17] C. Forssén, F. S. Dietrich, J. Escher, R. D. Hoffman, and K. Kelley, Phys. Rev. C **75**, 055807 (2007).
[18] B. Jurado *et al*., AIP Conf. Proc. **1005**, 90 (2008).
[19] S. R. Lesher *et al*., Phys. Rev. C **79**, 044609 (2009).
[20] J. M. Allmond *et al*., Phys. Rev. C **79**, 054610 (2009).
[21] R. Hatarik *et al*., Phys. Rev. C **81**, 011602(R) (2010).
[22] B. L. Goldblum, S. G. Prussin, L. A. Bernstein, W. Younes, M. Guttormsen, and H. T. Nyhus, Phys. Rev. C **81**, 054606 (2010).
[23] J. E. Escher and F. S. Dietrich, Phys. Rev. C **81**, 024612 (2010).
[24] N. D. Scielzo *et al*., Phys. Rev. C **81**, 034608 (2010).
[25] G. Kessedjian *et al*., Phys. Lett. B **692**, 297 (2010).
[26] S. Chiba and O. Iwamoto, Phys. Rev. C **81**, 044604 (2010).
[27] V. Zagrebaev and W. Greiner, J. Phys. G **31**, 825 (2005).
[28] V. Zagrebaev and W. Greiner, J. Phys. G **34**, 1 (2007); **34**, 2265 (2007).
[29] V. Zagrebaev and W. Greiner, Phys. Rev. Lett. **101**, 122701 (2008); J. Phys. G **35**, 125103 (2008).
[30] V. Zagrebaev and W. Greiner, Phys. Rev. C **78**, 034610 (2008).
[31] Y. Aritomo, Phys. Rev. C **80**, 064604 (2009).
[32] W. Hauser and H. Feshbach, Phys. Rev. **87**, 366 (1952).
[33] P. Fröbrich and R. Lipperheide, *Theory of Nuclear Reactions* (Clarendon Press, Oxford, 1996).
[34] V. I. Zagrebaev, A. V. Karpov, Y. Aritomo, M. A. Naumenko, and W. Greiner, Phys. Part. Nuclei **38**, 469 (2007); NRV codes for driving potential [http://nrv.jinr.ru/nrv/].
[35] G. F. Bertsch, Z. Phys. A **289**, 103 (1978); W. Cassing and W. Nörenberg, Nucl. Phys. A **401**, 467 (1983); A. Diaz-Torres, Phys. Rev. C **69**, 021603 (2004).
[36] J. Maruhn and W. Greiner, Z. Phys. **251**, 431 (1972).
[37] K. Sato, A. Iwamoto, K. Harada, S. Yamaji, and S. Yoshida, Z. Phys. A **288**, 383 (1978).
[38] Y. Aritomo and M. Ohta, Nucl. Phys. A **744**, 3 (2004).
[39] A. Karpov (private communication).
[40] J. Blocki, Y. Boneh, J. R. Nix, J. Randrup, M. Robel, A. J. Sierk, and W. J. Swiatecki, Ann. Phys. **113**, 330 (1978).
[41] J. R. Nix and A. J. Sierk, Nucl. Phys. A **428**, 161c (1984).
[42] J. Randrup and W. J. Swiatecki, Nucl. Phys. A **429**, 105 (1984).
[43] H. Feldmeier, Rep. Prog. Phys. **50**, 915 (1987).
[44] N. Carjan, A. J. Sierk, and J. R. Nix, Nucl. Phys. A **452**, 381 (1986).
[45] N. Carjan, T. Wada, and Y. Abe, in *Towards a Unified Picture of Nuclear Dynamics*, AIP Conference Proceeding No. 250 (AIP, New York, 1992).
[46] T. Wada, Y. Abe, and N. Carjan, Phys. Rev. Lett. **70**, 3538 (1993).
[47] T. Asano, T. Wada, M. Ohta, S. Yamaji, and H. Nakahara, J. Nucl. Radio Sci. **7**, 7 (2006).
[48] K. T. R. Davies, A. J. Sierk, and J. R. Nix, Phys. Rev. C **13**, 2385 (1976).
[49] Y. Aritomo, Nucl. Phys. A **780**, 222 (2006).
[50] A. N. Ignatyuk, G. N. Smirenkin, and A. S. Tishin, Sov. J. Nucl. Phys. **21**, 255 (1975).
[51] H. J. Krappe, J. R. Nix, and A. J. Sierk, Phys. Rev. C **20**, 992 (1979).
[52] K. Nishio, H. Ikezoe, S. Mitsuoka, I. Nishinaka, Y. Nagame, Y. Watanabe, T. Ohtsuki, K. Hirose, and S. Hofmann, Phys. Rev. C **77**, 064607 (2008).
[53] K. Nishio, H. Ikezoe, I. Nishinaka, S. Mitsuoka, K. Hirose, T. Ohtsuki, Y. Watanabe, Y. Aritomo, and S. Hofmann, Phys. Rev. C **82**, 044604 (2010).
[54] R. Bass, in *Nuclear Reactions with Heavy Ions* (Berlin, Springer, 1980), p. 265.
[55] W. U. Schröder and J. R. Huizenga, in *Treatise on Heavy Ion Science*, edited by D. A. Bromley, Vol. 2 (New York, Plenum, 1984), p. 140.
[56] K. Nishio *et al*., Phys. Rev. C **82**, 024611 (2010).
[57] M. Kamimura, M. Yahiro, Y. Iseri, Y. Sakuragi, H. Kameyama, and M. Kawai, Prog. Theor. Phys. Suppl. **89**, 1 (1986).
[58] S. Ayik, K. Washiyama, and D. Lacroix, Phys. Rev. C **79**, 054606 (2009).
[59] K. Washiyama, S. Ayik, and D. Lacroix, Phys. Rev. C **80**, 031602(R) (2009).
[60] B. Yilmaz, S. Ayik, D. Lacroix, and K. Washiyama, arXiv:1105.1946v1.
[61] A. V. Karpov, P. N. Nadtochy, D. V. Vanin, and G. D. Adeev, Phys. Rev. C **63**, 054610 (2001).
[62] T. Asano, T. Wada, M. Ohta, and T. Ichikawa, Prog. Theor. Phys. Suppl. **154**, 457 (2004).
[63] Y. Aritomo, S. Chiba, and K. Nishio (unpublished).